8/10/15/91 WG ①

# SANDIA REPORT

SAND91—1548 • UC—406
Unlimited Release
Printed July 1991

# Converting a Commercial Electric Direct-Drive Robot to Operate from Joint Torque Commands

Patrick F. Muir

**Prepared by**
**Sandia National Laboratories**
**Albuquerque, New Mexico 87185 and Livermore, California 94550**
**for the United States Department of Energy**
**under Contract DE-AC04-76DP00789**

DISTRIBUTION OF THIS DOCUMENT IS UNLIMITED

Issued by Sandia National Laboratories, operated for the United States Department of Energy by Sandia Corporation.

**NOTICE:** This report was prepared as an account of work sponsored by an agency of the United States Government. Neither the United States Government nor any agency thereof, nor any of their employees, nor any of their contractors, subcontractors, or their employees, makes any warranty, express or implied, or assumes any legal liability or responsibility for the accuracy, completeness, or usefulness of any information, apparatus, product, or process disclosed, or represents that its use would not infringe privately owned rights. Reference herein to any specific commercial product, process, or service by trade name, trademark, manufacturer, or otherwise, does not necessarily constitute or imply its endorsement, recommendation, or favoring by the United States Government, any agency thereof or any of their contractors or subcontractors. The views and opinions expressed herein do not necessarily state or reflect those of the United States Government, any agency thereof or any of their contractors.

Printed in the United States of America. This report has been reproduced directly from the best available copy.

Available to DOE and DOE contractors from
Office of Scientific and Technical Information
PO Box 62
Oak Ridge, TN 37831

Prices available from (615) 576-8401, FTS 626-8401

Available to the public from
National Technical Information Service
US Department of Commerce
5285 Port Royal Rd
Springfield, VA 22161

NTIS price codes
Printed copy: A03
Microfiche copy: A01

SAND91-1548 Distribution Category UC-406
Unlimited Release
Printed July 1991

# Converting a Commercial Electric Direct-Drive Robot To Operate from Joint Torque Commands

SAND--91-1548

DE92 000611

*Patrick F. Muir*

Intelligent Machine Principles Division
Sandia National Laboratories
Albuquerque, NM 87185

## Abstract

Many robot control algorithms for high performance in-contact operations including hybrid force/position, stiffness control and impedance control approaches require the command of the joint torques. However, most commercially available robots do not provide joint torque command capabilities. The joint command at the user level is typically position or velocity and at the control developer level is voltage, current, or pulse-width, and the torque generated is a nonlinear function of the command and joint position. To enable the application of high performance in-contact control algorithms to commercially available robots, and thereby facilitate technology transfer from the robot control research community to commercial applications, a methodology has been developed to linearize the torque characteristics of electric motor-amplifier combinations. A four degree of freedom Adept II robot, having pulse-width modulation amplifiers and both variable reluctance and brushless DC motors, is converted to operate from joint torque commands to demonstrate the methodology. The commercial robot controller is replaced by a VME-based system incorporating special purpose hardware and firmware programmed from experimental data. The performance improvement is experimentally measured and graphically displayed using three-dimensional plots of torque vs command vs position. The average percentage torque deviation over the command and position ranges is reduced from as much as 76% to below 5% for the direct-drive joints 1, 2 and 4 and is cut by one half in the remaining ball-screw driven joint 3. Further, the torque deviation of the direct-drive joints drops below 2.5% if only the upper 90% of the torque range is considered.



MASTER

## Table of Contents


**1. Introduction ..... 1**

**2. Prior Work ..... 3**

*2.1 Background ..... 3*

*2.2 End-Effector Force Feedback ..... 3*

*2.3 Motor Current Feedback ..... 4*

*2.4 Joint Torque Feedback ..... 5*

*2.5 Commutation Waveform Shaping ..... 5*

*2.6 Contributions of This Work ..... 8*

**3. A Practical Methodology for Linearizing Joint Torque ..... 8**

**4. Implementing Linear Joint Torque Commands On the Adept II Robot ..... 12**

*4.1 The Adept II Robot ..... 12*

*4.2 System Hardware ..... 12*

*4.3 System Firmware ..... 15*

**5. Experimental Results ..... 20**

*5.1 Dependence Upon Robot Calibration ..... 20*

*5.2 Choice of Ramping Function ..... 21*

*5.3 Performance Measures ..... 22*

*5.4 Torque Linearity Results ..... 24*

*5.5 Discussion ..... 25*

*5.6 An Unexpected Phenomenon ..... 31*

**6. Conclusions ..... 32**

*6.1 Summary ..... 32*

*6.2 Methodology Enhancements ..... 33*

*6.3 Continuing Work ..... 34*

**7. Acknowledgements ..... 34**

**8. Bibliography ..... 35**

# 1. Introduction

Model-based control of robot manipulators has progressed steadily over the past two decades. The earliest independent PID joint controllers were sufficient for pick and place maneuvers. However, the performances of these independent PID joint controllers were found to suffer from significant nonlinear and dynamic coupling forces/torques particularly at high speeds. The nature of these nonlinear and coupling forces/torques was discovered in the dynamic model of the manipulator.

Paul [Paul72] and Markiewicz [Markiewicz73] demonstrated that computation of robot dynamics within the control algorithm significantly reduced the effects of the nonlinear and coupling forces/torques and thereby linearized and decoupled the robot joint motions. Robot controllers based upon this *computed torque* or *inverse method* principle have demonstrated useful performance advantages over independent joint PID designs. The joint motor torques are computed in real-time and thus act as the command variables in computed torque algorithms. Several advanced robot control algorithms based upon the computed torque linearizing and decoupling methodology have since been introduced [Luh80, Yoshikawa88, Kuo90].

Ongoing research on the control of robots for in-contact tasks, such as automated assembly and light machining, demands increasingly more accurate command of joint torques. Advanced in-contact robot control algorithms [Whitney85] including stiffness control [Salisbury80], hybrid force/position control [Raibert81], and impedance control [Hogan84], have emerged utilizing joint torque as the commanded variable.

For in-contact tasks in which one or more degrees-of-freedom (dofs) are virtually motionless, any joint torque deviation is propagated directly to the point-of-contact thereby degrading task performance. Since torque deviations present an additional uncertainty within the robot control servo, reduced speed of operation must be accepted to maintain stability. Consequently, eliminating the uncertainties through torque linearization promises to increase the speed of in-contact operations. Another motivation for linearizing robot joint torque characteristics is to reduce torque ripple and thereby prevent excitation of structural vibrations. Thus, the linearity of the torque command capability of a robot is becoming crucial to high performance robot control. Future advances in robot

control for in-contact tasks depend heavily upon the ability to command accurately joint torques.

To develop and test the aforementioned high performance robot control algorithms, researchers have designed and built one-of-a-kind direct-drive manipulators which have provided command of motor torque [Asada85, Asada87] (although the torque linearity is seldom cited). Direct-drive is viewed as a necessary design feature for accurate torque command because the high frictions associated with geared drives dominate the torque transfer characteristics. Of the few, known commercial robots which are direct-drive [Curran85], none have torque command capabilities. Instead, the innermost control variable accessible to the user is joint position or velocity; and the innermost control variable accessible to the robot control engineer is either motor voltage, current or pulse-width. Because command of joint torques is required, implementing the algorithms directly on commercially available robots presents a formidable challenge. Thus, the transfer of robot controller technology from research to the commercial and industrial sectors is seldom accomplished.

In this paper, a commercial robot, the Adept II, is equipped with joint torque command capabilities through the application of special purpose hardware and firmware. The approach applies directly to any direct-drive robot utilizing electric motors and amplifiers, and joint position sensors. Considerable effort has been directed towards enabling commercial application of the approach by automating the experimental data collection aspects to minimize manpower requirements and human error.

The remainder of this paper is organized as follows. In Section 2, the prior work in the area of torque control of electric motors and its application to robotics is summarized. The contributions of the present work are also enumerated and contrasted with the prior work. The methodology for linearizing joint torque characteristics for a robot with electric motors and joint position encoders is described in Section 3. Then, in Section 4, the methodology is applied to the Adept II robot. In Section 5, experimental data from the Adept II joint torque command implementation is presented and discussed. Section 6 concludes the work with a summary of the promising results, the potential for improving robot performance and some possible enhancements to the methodology.

## 2. Prior Work

### *2.1 Background*

Typical high torque electric motors applied in robot designs are direct current torque motors, brushless DC torque motors and variable reluctance motors [Asada87]. Each motor is accompanied by an amplifier which is matched to the motor's particular current and voltage characteristics. All of these motor-amplifier combinations experience torque ripple due to the saliency of the motor construction (variable reluctance motors in particular). The servo-disc motor [PMI88], as yet rarely applied in robotics, is currently the only known motor design which claims to provide zero torque ripple.

The key technology required for the conversion of a commercial robot to operate from joint torque commands is the approach to commanding linear joint motor torques. In this context, linearization ideally means having zero torque ripple (the torque is constant with changing position) and an identical correspondence between commanded torque and actual torque (the actual torque is linear with the torque command at constant position). Existing approaches to joint torque linearization fall into four categories:

1) End Effector Force Feedback;
2) Motor Current Feedback;
3) Joint Torque Feedback; and
4) Commutation Waveform Shaping.

Each approach is summarized below. The methodology of this paper falls into the Commutation Waveform Shaping category.

### *2.2 End-Effector Force Feedback*

When robot position control algorithms, which performed admirably in free space, were found to be unusable in-contact, the robot control community turned to force control algorithms for improved performance. The natural first attempt at force control was to apply end-effector force feedback to servo the robot while in-contact. One implementation of end-effector force feedback [Whiney85] is diagrammed in Figure 1. In this class of control algorithms, the Jacobian transpose and/or the Jacobian inverse is applied in one of two positions. It either appears in the feedback path to compute the joint torques from the end-effector force/torque sensor measurements (as diagrammed) or it appears in the feedforward path to convert Cartesian-space forces/torques into joint-space. The joint or Cartesian-space feedback values are

combined with the respective joint or Cartesian-space commands and then processed through a torque regulator to adjust the amplifier inputs.

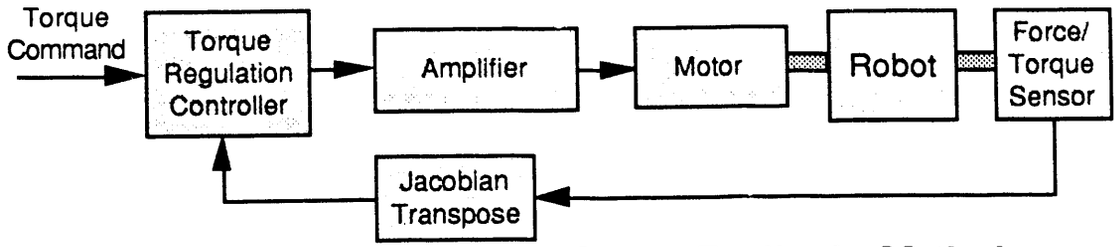


**Figure 1: End-Effector Force Feedback Method**

Several problems with End-effector force feedback methods surfaced including: computational and sensor delays, non-colocation of actuators and sensors, effects of kinematic and dynamic modeling errors, and unmodeled dynamics due to the flexibility of the arm. These destabilizing effects lead control engineers to develop the following three joint torque command approaches. A high performance robot controller is expected to result from the *combination* of this robot-level approach with one or more of the following joint-level torque linearization methods

*2.3 Motor Current Feedback*

The Motor Current Feedback approach [Asada87] is the most commonly applied method of torque linearization providing reasonable performance for direct current (DC) torque motors and brushless DC motors. In this method, the amplifier senses the current delivered to the motor and a current servo loop is closed within the amplifier as a means of regulating torque. This approach works well for motors in which the torque is closely proportional to the applied current independent of position. Although a linear relationship between motor torque and applied current is widely assumed in the robotics literature, it is not an accurate assumption for variable reluctance motors and is only accurate to first order for brushless DC motors. For high performance operation, as is required for in-contact tasks, and for some new motor designs (variable reluctance motors in particular) the linear torque-current relationship is not a sufficiently accurate model.

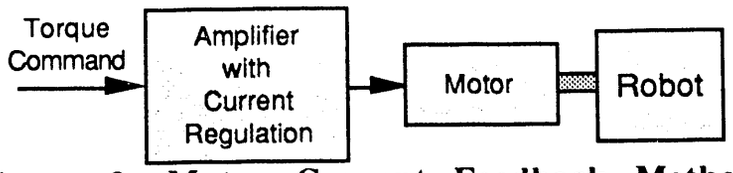


**Figure 2: Motor Current Feedback Method**

The motor current feedback method is diagrammed in Figure 2. The current feedback and the servo adjustments typically occur within the motor amplifier.

*2.4 Joint Torque Feedback*

Joint torque regulation has also been achieved using the torque feedback approach [Asada85, Pfeffer86] as diagrammed in Figure 3. The joint torque is measured directly at the motor shaft. The measured joint torque is compared with the torque command. Torque regulation is based upon the error between the commanded and actual torque.

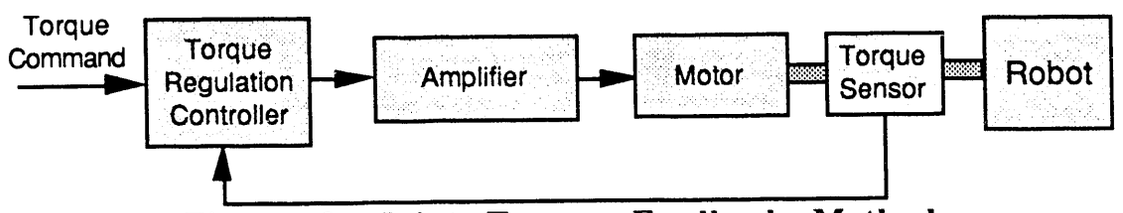


**Figure 3: Joint Torque Feedback Method**

This approach eliminates the problems of non-colocated sensors and actuators, and unmodeled arm dynamics. It has been demonstrated to significantly reduce the effective joint friction Luh83]. The disadvantages of this approach include the difficulty of mounting torque sensors in an existing mechanical structure and the added control difficulties associated with adding a flexible element to the driving structure.

*2.5 Commutation Waveform Shaping*

In contrast to the prior three methods, commutation waveform shaping is a *feedforward* approach. In this method, the torque command and the current motor position are applied to index into a precomputed table and retrieve the proper motor actuation values. The commutation waveform shaping method is diagrammed in Figure 4.

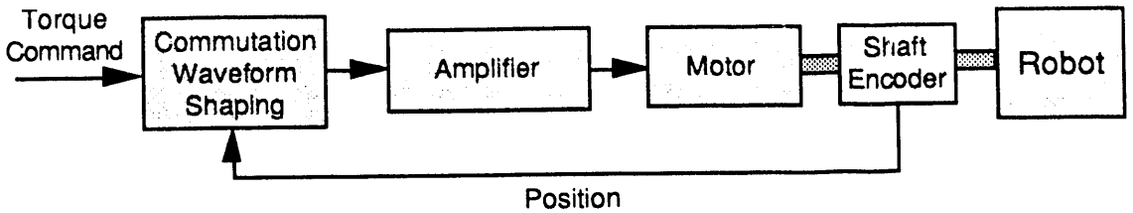


**Figure 4: Commutation Waveform Shaping Method**

The Commutation Waveform shaping method is seen as the only practical choice for converting the Adept II to obtain a joint torque command capability. The end-effector feedback approach alone is not sufficient for high performance in-contact robot control as described in Section 2.2. It is exceedingly difficult to mount force sensors on the existing joint structure of the Adept II for implementing joint torque feedback method. Finally, the variable reluctance motors on joints 1 and 2 have highly nonlinear current-torque relationships, thus eliminating the motor current feedback method.

Within the available literature on commutation waveform shaping most attempts have followed the approach of applying either a trapezoidal or sinusoidal waveform to the motor phases and optimizing the switching times to reduce torque ripple. This approach is simple but inadequate for high accuracy torque generation because the actual waveform necessary to zero the torque deviations (especially for a variable reluctance motor) is significantly different then either a trapezoid or a sinusoid [Wallace90b] (also see Section 5).

An advanced waveform shaping method is described in [Ish-Shalom89]. The hardware of this method energizes the motor phases of a step motor to implement a relatively constant torque. A PD control law and compensation for motor torque vs current nonlinearities are implemented in a control law applied at a higher level. No attempt was made to compensate for the torque variations of an individual phase with changing position.

A linearizing and decoupling transformation (LDT) approach to commutation waveform shaping was introduced in [Taylor88] for the purpose of simplifying the control of a variable reluctance motor to act like a DC motor. For the LDT approach, the commutation waveform shape was not selected a-priori, but is identified by collecting motor data through experimentation. In [Taylor88], the motor torque data is fit to a multivariable function, solved for the actuation value in terms of position and torque command, and stored in digital memory EPROM. The EPROM is applied within a specially built digital system at high clock rates to determine the actuation

values for the current motor position and torque command. In this way the model of the motor torque characteristics is applied within the feedforward path of the system to linearize the motor torque characteristics. The LDT shows great promise for linearizing nonlinear motor characteristics in much the same manner that the computed torque control approach linearizes the control of robot nonlinearities; by applying the inverse model of the nonlinearity directly within the system.

Some deficiencies of the original LDT approach include the following. No experimental torque linearity results were cited. Only single phase characterization was completed. Thus, it was assumed that all phases had identical torque generating characteristics, which is not an accurate assumption. Also, the assumption that the total torque is the superposition of the torques of the three phases is inaccurate in the phase transition region. The data were collected while the joints were moving by using a separate motor driven fixture. The approach was developed exclusively for variable reluctance motors.

The application of the LDT was simulated in [Wallace90a] to demonstrate torque ripple variations with speed. Although the source of speed dependency is not described, torque ripple is demonstrated to increase with speed in simulations of motor motions above 500 rpm. This is a higher speed range than is expected in direct-drive robot applications. Simulations of the LDT approach were also conducted in [Wallace90b] to balance the commutator of variable reluctance motors. In this work, the peaks and rates of change of the actuation values are reduced by proper assignment of the commutator ramping function.

The LDT approach was applied to the control of the AdeptOne robot in [Vertal89]. The motivation for this work was the requirement for joint torque command capabilities for in-contact force controlled robot applications. The AdeptOne is essentially the same robot as the Adept II (which is utilized in the present work) except that joint 2 is driven by its motor through a steel band, rather than a four-bar linkage. Special-purpose joint interface boards were built to implement the LDT methodology. Experimental results were presented for a few specific command values on one motor. Single phase characterization and a motor driven device for data collection was employed.

This work was followed closely by [Patel90] and [Newman91]. Improved torque control results were obtained for joints 1 and 2, and PD control algorithms were developed for joints 3 and 4. Experimental results were presented for a selected set of commands

for joints 1 and 2. Single phase characterization and a stepper motor driven platform were applied.

Work on the linearization of joint torques with the LDT approach at Sandia National Laboratories has been ongoing simultaneously with the previously cited works. In particular, [Starr90] documents prior work conducted. The LDT approach was implemented on joint interface boards to linearize the torque command of an Adept II robot. This work utilized single-phase in-motion manual characterization, elaborate data collection fixtures, and fitting to a multivariable function. The procedure was applied to joints 3 and 4, but experimental results for the brushless DC motors were not obtained.

### *2.6 Contributions of This Work*

The present work is an application of the LDT commutation waveform shaping approach representing three major improvements over the previous works. Firstly, the approach has been generalized into a methodology which applies to any electric motor/amplifier combination having position feedback. In this paper, successful application of the methodology is demonstrated on both variable reluctance and brushless DC motors using amplifiers of unknown transfer characteristics. Secondly, The experimental procedure for look-up table generation is greatly simplified and completely automated. The data collection process for each joint is automated such that no manual operations are required, and no motor driven or elaborate fixtures are required. Thirdly, the data collection procedure is more accurate and complete. In the phase transition regions, data are collected with two phase excitation. The data are collected under static conditions ensuring sufficient time to acquire accurate force readings. The data collection for look-up table generation and for verification of results is complete in the sense that high density data is collected for the entire position and command range considered. Thus, the tables are derived from a higher density of actual data and the results can be shown graphically for the complete position and command ranges in 3-dimensional plots. These improvements ease data collection to enable commercial application and improve performance.

## 3. A Practical Methodology for Linearizing Joint Torque

The present joint torque linearization methodology is based upon the linearizing and decoupling transformation developed in

[Taylor88]. Here, the approach is generalized, and the specifics of hardware implementation and experimental data collection are improved providing significant advantages in terms of ease of implementation and performance.

The central component of the joint torque linearizing methodology is a look-up table. The look-up table stores the torque generating characteristics of the joint motor as a function of *position*, *command* and *phase number*. For the purpose of this discussion, a brushed electric motor has only one phase, because it has only one control input, while a brushless electric motor typically has 3 phases corresponding to the 3 control inputs. The present methodology applies to both brushed and brushless electric motors.

The look-up table is applied as follows. The current motor position, torque command and a phase number are applied to form the table address, which is used to index into the look-up table and retrieve the motor actuation value (e.g., the pulse-width to apply). If the actuation values for all phases are retrieved and applied simultaneously, the motor will generate the commanded torque until the joint position changes. The table look-up and control value application must be repeated at a high rate to obtain a smooth torque output while in the motor is in motion.

In general, without delving into the details of motor operation, electric motor torque varies periodically with position and increases monotonically with the actuation value. The exact shapes of these relationships will depend upon the specific motor. For a complete view of the motor torque as a function of position and command value, we can use a three-dimensional plot. We present the torque plot in Figure 5 of the joint 2 variable reluctance motor on the Adept II robot as an example. The torque data plot graphically displays the motor's torque variations with position and pulse-width. Note that the position range covers one complete actuation cycle of the motor; many (150) actuation cycles are required to rotate this motor one complete revolution.

To obtain linear torque behavior from this motor, we must simultaneously compensate for the non-linear periodic nature of the position dependencies and the non-linear exponential nature of the command value dependencies. Specifically, the look-up table shown in Figure 6 is required. Note that the look-up table has "hills" at the positions where the motor characteristics have "valleys". This *inverse model* displays the basic principle underlying the joint torque linearization methodology.

# Joint 2 Look-Up Tables: Narrow Ramping Function

## Figure 5: Torque Data

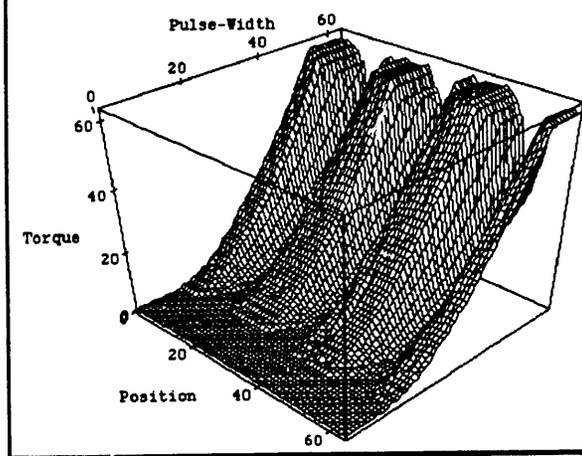


**Legend for Data**

Pulse-Width Scale: 1=1/128% Duty Cycle
Torque Scale: 1=81 oz in
Position Scale: 1=1/64 of Full Cycle

## Figure 6: Look-Up Table

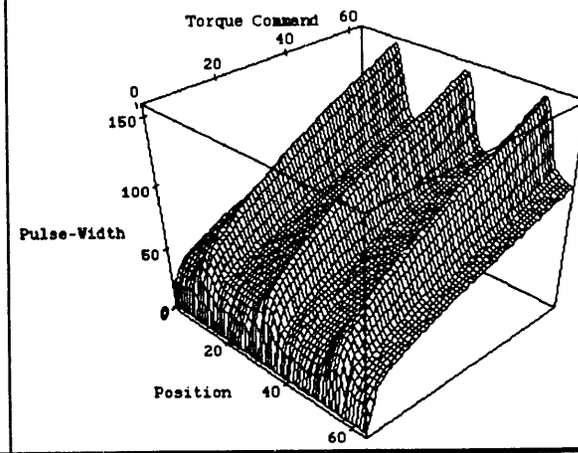


**Legend for Look-Up Tables**

Torque Command Scale: 1=62 oz in
Pulse-Width Scale: 1=1/256% Duty Cycle
Position Scale: 1=1/64 of Full Cycle

## Figure 8: Individual Phase Look-Up Tables

### Phase 1

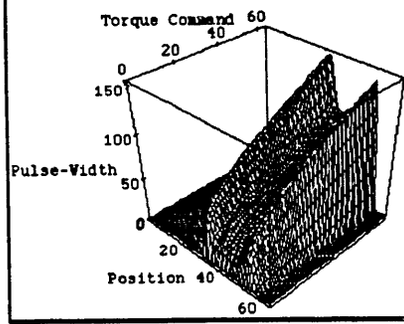


### Phase 2

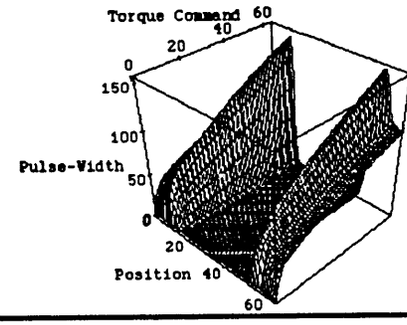


### Phase 3

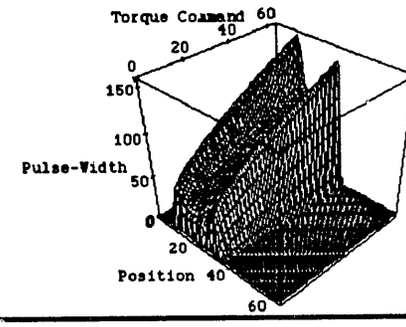

The motor *commutation* must also be programmed into the look-up table. The commutation must ensure that the proper motor phases are energized while the inverse model is simultaneously implemented. If we were simply to switch from one phase to another at the proper positions, this would be a straightforward matter. However, we must make the transition from one phase to the next gracefully by ramping down the preceding phase and ramping up the current phase to avoid large torque deviations in the transition region. The transition region width and the exact shape of the ramping function are free to be chosen.

A typical transition ramping function for a three-phase electric motor in one direction of motion is shown in Figure 7. We will refer to this function as the *narrow* trapezoidal ramping function. The position range for one actuation cycle, the sequence of phases (1-2-3 or 3-2-1), and the positions of the transition regions will depend upon the particular motor. The ramping functions indicate which phases are to be energized at each motor position and their relative proportions. There are three single-phase regions, where only one phase is energized, and three transition regions, where two phases are energized with the proportions specified by the ramping function.

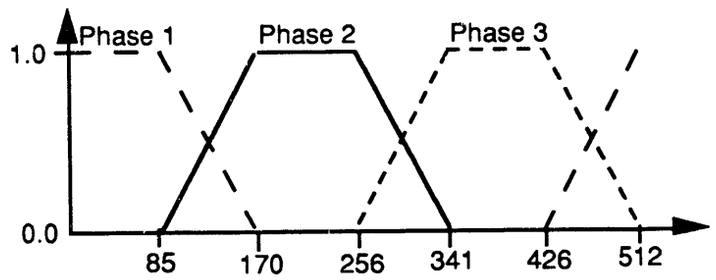


**Figure 7: Narrow Trapezoidal Ramping Function**

Once the transition ramping function is defined, the table look-up process can be viewed in three steps:

(1) The inverse model look-up table (e.g., Figure 6) is applied to retrieve the actuation value (pulse-width) required at the current position and current torque command;

(2) The actuation proportion for each of the motor phases is retrieved from the ramping function (e.g., Figure 7) at the current position; and

(3) The actuation value for each motor phase is computed by multiplying the actuation value obtained in Step (1) by the respective actuation proportion obtained in Step (2).

With this understanding of the operation of the methodology, we can condense all three steps into one step by using multiple look-up tables, one for each phase. To make the look-up table for a particular phase, simply multiply the inverse model with the actuation proportion of that phase for all positions and commands. In this way, the preceding *sequential 3-step* process having one inverse model look-up table can be implemented as a *parallel 1-step* process having m look-up tables, where m is the number of motor phases (for the Adept II robot, m=3). The three phase look-up tables for the joint 2 motor using narrow trapezoidal ramping are plotted in Figure 8.

## 4. Implementing Linear Joint Torque Commands On the Adept II Robot

### *4.1 The Adept II Robot*

To demonstrate and evaluate the joint torque linearization methodology described in Section 3, we have applied it to the Adept II robot manipulator. The Adept II is a commercial SCARA robot having 4-dofs in the standard configuration. Joints 1 and 2 are rotational joints actuated by 3-phase variable reluctance motors. Motor 1 actuates joint one directly and motor 2 actuates joint 2 through a rigid 4-bar linkage. Joints 3 and 4 are actuated by 3-phase brushless DC motors. Motor 3 actuates translational joint 3 through a ball screw and motor 4 actuates rotational joint 4 directly by means of a pin-in-slot mechanism. Note that joints 1, 2 and 4 are not geared and thus direct-drive. Joints 1, 2 and 4 and motor 3 have optical shaft encoders for position feedback. The motor amplifiers accept 40 Khz TTL-level pulse-width modulated signals and apply 110 volt DC actuating signals to the motors. The amplifier transfer characteristics from the input pulse-width to the output motor current (or voltage) are unknown. By design, the torque linearization methodology does not require a-priori knowledge of the amplifier transfer characteristics.

### *4.2 System Hardware*

The table look-up for each joint motor is implemented by a combination of special-purpose hardware, specifically a Joint Interface Board (JIB), and firmware. The entire robot system in the JIB-control configuration is depicted in Figure 9. The inputs to the motor amplifiers are wired to the JIBs as the source of motor commands. The position encoder signals from the robot are also

wired to the JIBs for joint position feedback. The four JIBs are constructed on standard VME bus compatible circuit boards.

A Heurikon HK68/V3E CPU board with a 68030 microprocessor and a 68882 floating point co-processor act as the robot controller. The control and data collection code is written in C and compiled on the Sun 4-330 workstation. A Communications Machinery Corporation Ethernet Node Processor (ENP-10) allows control and data collection code to be downloaded from the Sun. The control algorithms for the CPU are the topic of on-going research and thus are beyond the scope of the present discussion. A Lord 6-axis force/torque sensor with 30 lb force and 100 in-lbs torque ranges is mounted at the robot end effector for motor characterization experiments. Access to the force/torque measurements is achieved by the CPU via a Force SYS68K PIO-1 Parallel I/O card which also resides on the VME bus.

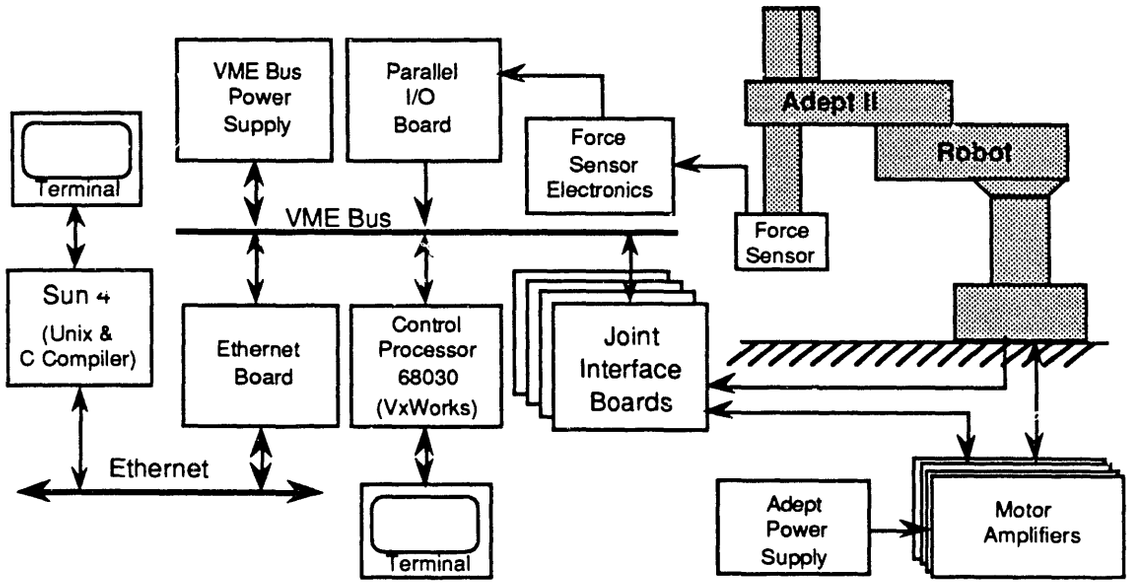


**Figure 9: Laboratory System Interconnect**

The functional operation of a JIB is diagramed in Figure 10. The heart of each board consists of three EPROM memory chips, one to implement the look-up table for each motor phase. Each look-up table is organized as a 128K x 8 data array. The motor position (9 bits, unsigned) and the torque command (8 bits, signed) are concatenated to form the table address. The 8 bit unsigned content of the table is the pulse-width actuation value for the motor amplifier.

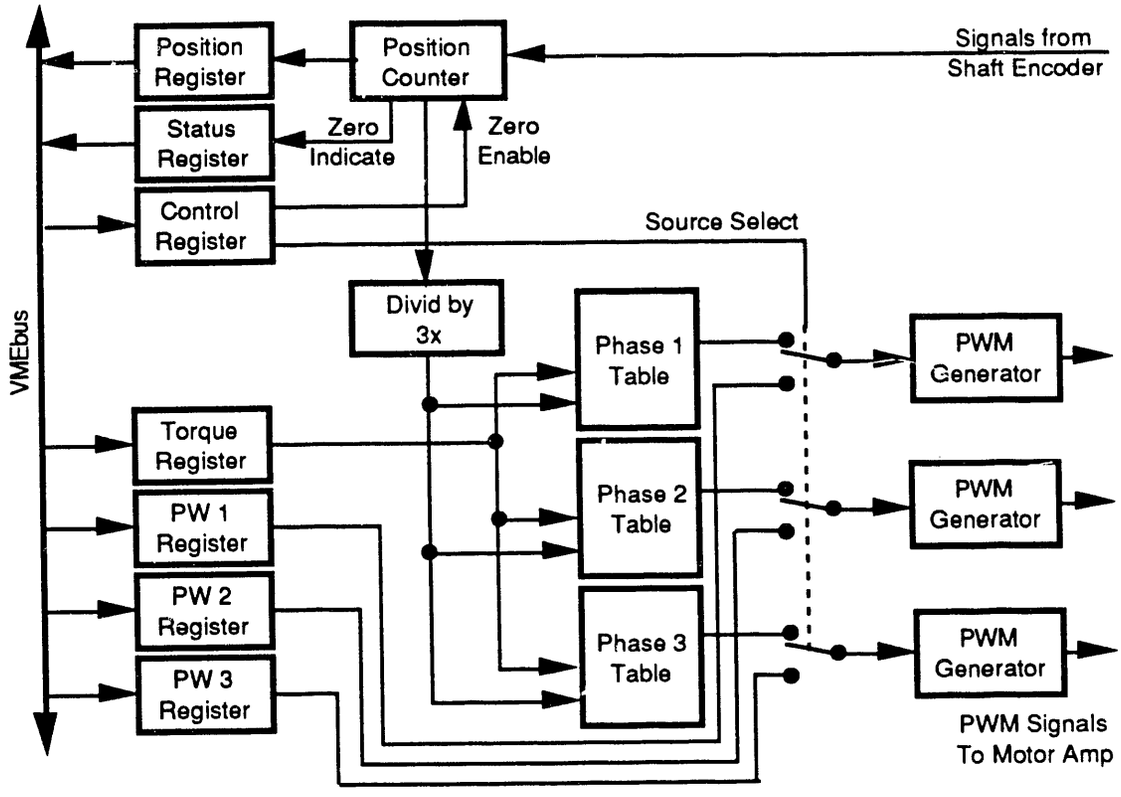


**Figure 10: JIB Functionality**

Additional circuitry is provided on the JIB to handle:

* Counting the shaft encoder pulses to keep track of the motor position;
* Providing access to the motor position from the VME bus;
* Dividing the motor position by a multiple of 3 (depending upon the particular motor) so that the least significant 9 bits of position repeat with a period that corresponds to the period of the motor actuation cycle;
* Generating a 40 Khz PWM signal for the motor amplifier;
* Allowing the position counter to be zeroed from the VME bus for robot calibration;
* Providing a flag, readable from the VME bus, that indicates when a zero index is detected by the shaft encoder; and
* Allowing the application of a pulse-width to each motor phase from the VME bus for experiments.

All communication between the control CPU and the motors and shaft encoders is accomplished by reading from or writing to memory locations located on the JIBs. By this means, a control algorithm running on the CPU may: command a pulse-width from

any phase of any joint motor, command a torque from any motor (when the look-up tables are installed), or command the position counter to zero when a zero index occurs; by simply writing the appropriate values to specific memory locations. A control algorithm may also: read the position of any joint or read the shaft encoder zero status of any joint; by simply reading specific memory locations.

*4.3 System Firmware*

The crucial component of the joint torque linearizing implementation is its firmware: i.e., the content of the EPROM look-up tables. The content of a phase look-up table represents the inverse motor torque characteristics which are scheduled according to the transition ramping function for the particular phase as discussion in Section 3. The first step towards computing the look-up tables for a joint is to identify the motor torque characteristics. An experiment must be conducted for each joint which gives the torque vs position vs command characteristics.

It is not practical to attempt to acquire a complete set of motor characterization data because of the large volume required. For example, with the table position quantized to nine bits ($2^9=512$ different values), and the command quantized to 8 bits ($2^8=256$ different values), we would need to collect $2^{17}=131,072$ torque measurements for each motor. If each measurement took just 1 second, the entire data acquisition process for one motor would take in excess of 36 hours. Since this is impractical, we have designed an experiment to collect data samples at evenly spaced positions and commands. The interstitial torque values are then easily interpolated. Even at the reduced volume of data, the tedium of the collection experiment makes automation of the task a necessity.

We have devised the following experimental procedure for automating the collection of data for a joint x, where $x \in \{1,2,3,4\}$. First, a constraint is fixed within the robot workspace such that: (1) when data is being collected, only the torque of joint x affects the end-effector force/torque measurement; and (2) The position of joint x while it is against the constraint can be systematically stepped through the entire table position range (i.e., one actuation cycle) by incremental motions of another joint $y \neq x$. The set of four different constraint configurations shown in Figure 11 was applied to obtain the data sets for the 4 joints respectively.

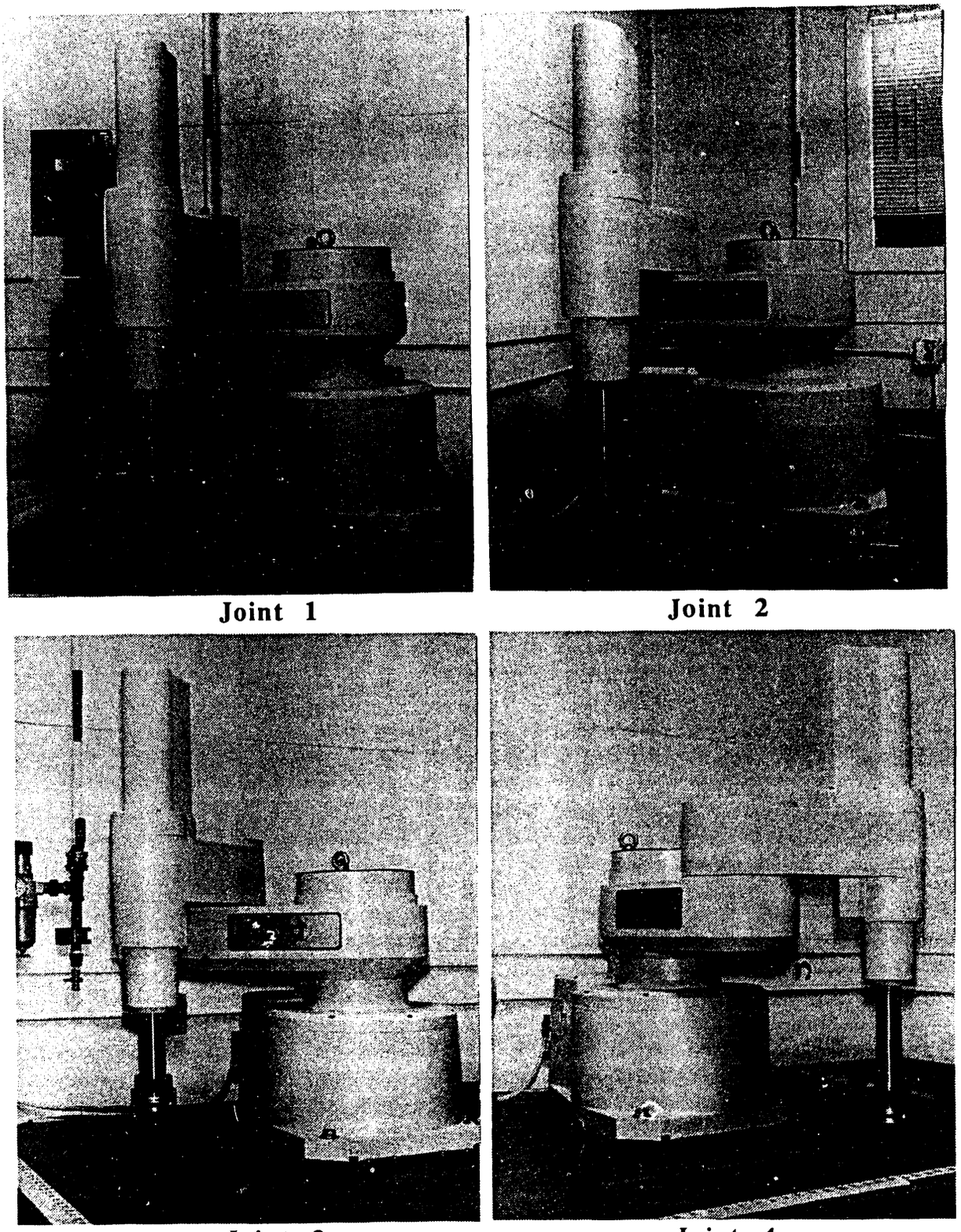

Joint 1 Joint 2

Joint 3 Joint 4

Figure 11: Data Collection Configurations

For joints 1, 2 and 3, an inclined metal constraint is applied to enable systematic changes of position. For example, the position of joint 1 can be systematically stepped through a complete actuation cycle by incremental motions of joint 3 as shown in the "Joint 1" photo. In this case, joint 1 is termed the *primary* joint, and joint 3 is the *secondary* joint. Similarly, joint 2 is the primary joint and joint 3 is the secondary joint when collecting the data for joint 2. To collect data for joint 3, joint 2 is held stationary (by energizing one of its phases), joint 3 acts as the primary joint and joint 1 acts as the secondary joint. A tongue-in-groove setup is utilized to collect data for the rotational joint 4. By freeing joint 2 and incrementally moving the secondary joint 1, the position of the primary joint 4 can be systematically stepped through an actuation cycle.

The data collection procedure mainly consists of two hierarchical loops as shown in the flowchart of Figure 12. The inner loop steps the pulse-width command from 0 up to the maximum pulse-width or until the force sensor saturates, whichever occurs first. At each pulse-width application, the end-effector position is allowed to settle and 10 force measurements are taken and averaged, to minimize the effects of noise, and then stored. The outer loop steps the position through a complete actuation cycle by proper control of the secondary joint. Notice that the force/torque biases are measured, stored and subtracted from the force/torque measurements at each position. This has the additional effect of removing gravity from the data for joint 3 since gravity is seen as a force/torque bias. Although the data collected is spaced relatively evenly throughout the position and command ranges, friction and nonlinear kinematics in the system preclude exactly even spacing of the data. The joint torque linearization methodology has proved to be insensitive to these moderate spacing variations.

Within the inner loop, the position of the end-effector changes during the data collection process because of the increasing forces and the compliance of the robot and force sensor. However, this presents no problem, since each pulse-width application is obtained from the ramping function according to the *current* motor position and each force measurement is stored using the *current* motor position. The data collection experiment requires nominally 4 hours for each joint.

Once the data (consisting of triplets: position, pulse-width and torque) for the joint has been acquired, the inverse model of the motor can be easily generated. Data conversion is accomplished off-line one element at a time. First, the torque is scaled so that the largest torque measurement maps into the largest torque index (i.e.,

255). Then, the pulse-width is stored at the table address formed by concatenating the scaled torque with the position.

At the low end of the pulse-width command range, during the conversion from experimental data into the look-up table, there are typically sets of pulse-widths which map into the same torque value in the look-up table due to quantization of the torques. If we were simply to step successively through the data, mapping each into the look-up table, the last pulse-width to map into a particular torque would always remain. It is more appropriate that the median pulse-width within the set remains. To enable this, when more than one pulse-width maps to the same torque value, we map only the median pulse-width value in the set.

So far, the original evenly spaced data has been converted to the inverse model look-up table producing evenly spaced entries. Now the remainder of the look-up table can be generated by interpolation. The form of interpolation applied is not important (linear interpolation is used) because the difference between two values being interpolated between is typically small. Interpolations occur along constant position contours as well as constant torque contours. Smaller voids are always filled by interpolation before larger ones. To generate a particular phase look-up table from the inverse model look-up table, we simply multiply each element of the inverse model look-up table by the phase proportion for that element and phase from the transition ramping function.

It is important to understand that the phase transition ramping function allows the collection of data with two phases energized in the transition regions. The ramping function registers the collected data with the final look-up tables in the following way. Within the data collection procedure, the ramping function is consulted before each pulse-width application and force data measurement. The current position is measured and used to index into the ramping function to determine which phases to energize at what proportions. The measured force is stored under the current position. Later, when the individual phase look-up tables are being generated, the ramping function is again consulted before each look-up table entry is computed. The look-up table position is applied to index into the ramping function to determine which phases were energized and at what levels in order to obtain the current torque value. In this way, the phase contributions are apportioned in the look-up tables exactly as they were during the data collection. Consistent application of the phase transition ramping function is a primary factor in obtaining accurate joint torque command results.

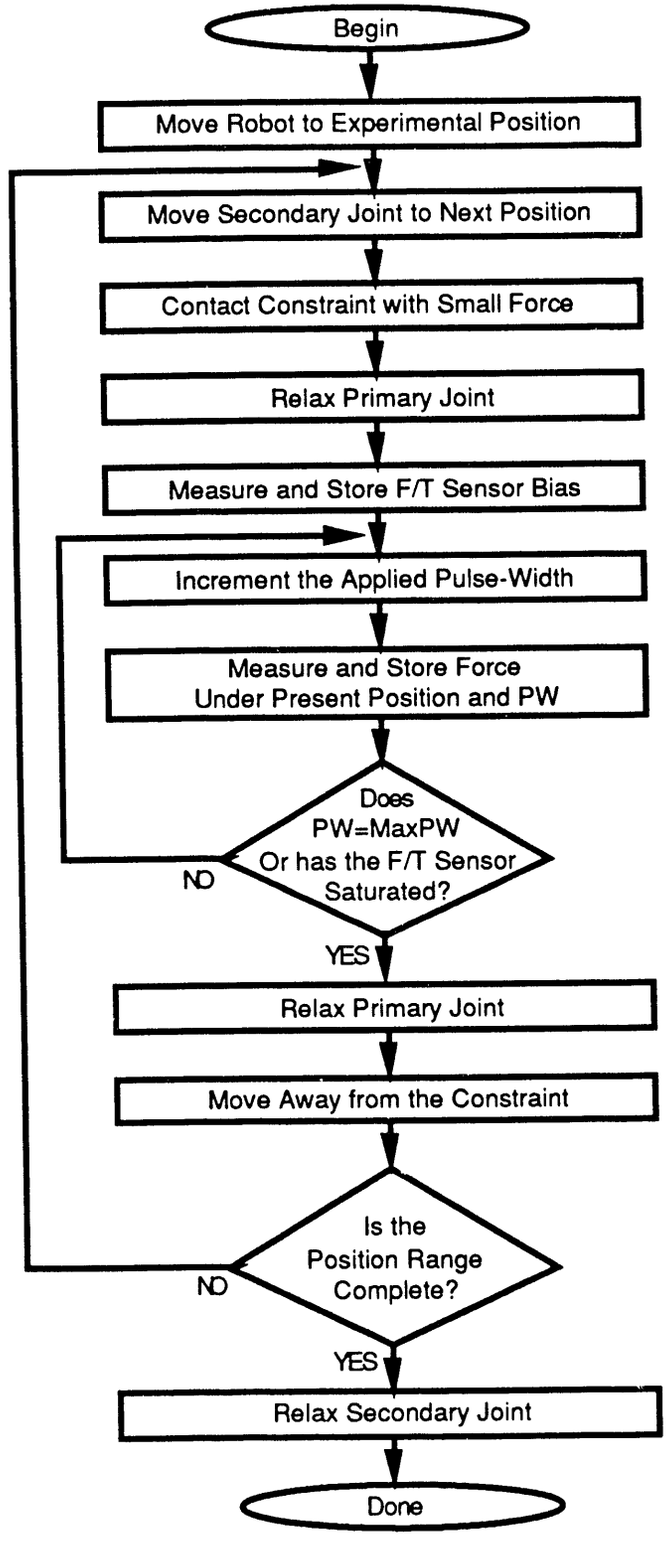


**Figure 12: Data Collection Flowchart**

We have thus far considered acquiring data and computing the look-up tables for *one* direction of torque. For the opposite torque direction, the reverse phase sequence is required. By close examination of motor operation, it is found that the correct command values for the opposite direction can be derived by reflecting the original phase look-up tables about their respective equilibrium positions. The equilibrium position $e_i$ is the table position resulting when phase i is energized and the motor motion is allowed to settle. For example for phase i, if a pulse-width s is required to attain a torque $\tau$ at position p then the same pulse-width s is required to command the opposite torque $-\tau$ at position $\{[e_i + (e_i - p)] \; mod \; 512\}$ After the look-up table for a phase has been assembled for one torque direction, the second half of the look-up table corresponding to the opposite torque direction is assembled using this mapping. The most accurate approach would be to take data for both torque directions. However, for the Adept II, there are no convenient data collection configurations (similar to those in Figure 11) which allow collection of data in the opposite torque direction for joints 1, 2 and 3.

## 5. Experimental Results

### *5.1 Dependence Upon Robot Calibration*

Since the Adept II utilizes incremental optical shaft encoders for position feedback, the robot must be calibrated each time the power is turned on to initialize absolute position references. Since we replaced the commercial controller with a self-contained system, we also had to develop the calibration (or homing) program. During calibration, each joint of the robot must be moved past its hardware zero position and the hardware position counters must be initialized to zero when the zero pulse is detected. This calibration program, above all, must be repeatable. Since our motor characterization data is position dependent, it is important that the position values measured during the data collection experiments are the same as those measured when the robot is later utilizing the look-up tables in torque command mode. Joint torques cannot be commanded prior to robot calibration. The calibration program was developed and debugged using the pulse-width mode of joint command.

To ensure that the calibration program was repeatable, the following experiments were conducted. First, the repeatability of manually positioning the robot in a reference posture (against its internal hard-stops) was measured by repeating the task 10 times

and recording the resulting joint positions. The standard deviation of these measurements gives us a measure of repeatability of the manual placement task. The smaller the standard deviation, the higher is the repeatability. The same experiment was conducted 10 times using the software calibration program *before* each of the manual placements. We would expect that if the calibration program were not repeatable, the measured joint positions would not be consistent, and the standard deviation of the second set of experiments would be larger than that of the first.

The results are tabulated in Table 1. If we use the standard deviations of the first experiment as references, the average percent standard deviation over all four joints during the second experiment is 79% and thus slightly less. We have therefore concluded that the software calibration program *is repeatable* and sufficient for continuing into the data collection portion of this project.

Table 1: Homing Results

| | J1 | J2 | J3 | J4 |
|---|---|---|---|---|
| Standard Deviation without Homing | 0.0077 | 0.0226 | 0.0117 | 0.2646 |
| Standard Deviation with Homing | 0.0062 | 0.0267 | 0.0036 | 0.2278 |
| Relative Percentage Standard Deviation | 81% | 118% | 31% | 86% |
| Average Percentage | 79% | | | |

*5.2 Choice of Ramping Function*

The narrow trapezoidal ramping function was initially applied in this work following the prior work of Starr and Wilson [Starr90]. The motor torque characteristics and look-up tables resulting have been introduced in Section 3 and plotted in Figures 5, 6 and 8. Notice the deep valleys in the torque vs pulse-width data. The bottom of the lowest valley represents the largest torque which can be obtained independent of position and thus limits the torque range of the joint torque linearization results. For joint 2 this torque limit is only 3966 oz in.

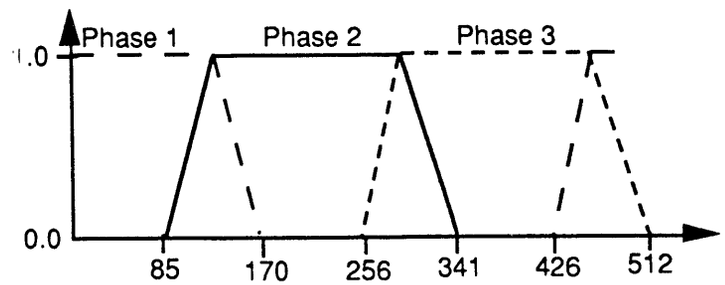


**Figure 13: Wide Trapezoidal Ramping Function**

In an effort to increase the torque range of the results, the *wide trapezoidal ramping function* depicted in Figure 13 was implemented. Since each phase remains at 100% for a wider position range, the wide trapezoidal ramping function showed promise to increase the motor torque in the phase transition region where the original valleys were identified. The motor torque characteristics and look-up tables for the wide trapezoidal ramping function for joint 2 are plotted in Figures 14 to 16. The valleys in the wide trapezoidal torques are not as deep as when the narrow ramping function was applied. Here, the deepest valley occurs at 5546 oz in. Thus, by applying wide trapezoidal ramping, the resulting torque range has been increased 40%.

Notice also the large command excursions required from each phase in Figure 8 for implementation of narrow ramping; whereas, the phase commands for wide ramping in Figure 16 are much smoother. This result is analogous to balancing the commutator of the motor as has been developed in [Wallace90b]. The three remaining joints displayed similar torque range extensions and command smoothing when wide trapezoidal ramping was applied. For the remainder of our discussions, we will apply wide trapezoidal ramping exclusively.

### *5.3 Performance Measures*

To graphically view the improvement in motor torque linearity, we compare the three-dimensional "before" plot of torque vs position vs pulse-width with the "after" plot of torque vs position vs torque command. The data for the after plot has been acquired for each joint from an experimental procedure nearly identical to that described in Section 4.3 for collecting the motor torque characteristics. The two differences being that the look-up tables are utilized and, instead of incrementally stepping up the pulse-width at each motor position, the torque command is incrementally stepped up.

The performance of the torque linearization methodology is measured quantitatively in terms of average percent magnitude deviation (APMD). The overall APMD is defined as:

$$\text{Overall APMD} = \frac{1}{PC} \sum_{c=1}^{C} \sum_{p=1}^{P} \frac{|\tau_d(p,c)-\tau(p,c)|}{|\tau_d(p,c)|} \qquad (1)$$

# Joint 2 Look-Up Tables: Wide Ramping Function

## Figure 14: Torque Data

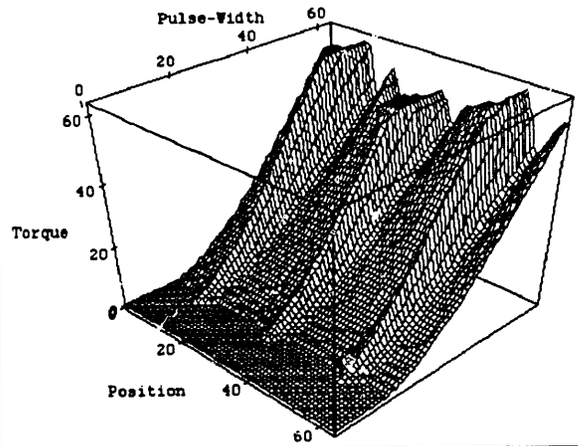


**Legend for Data**

Pulse-Width Scale: 1=1/128% Duty Cycle
Torque Scale: 1=114 oz in
Position Scale: 1=1/64 of Full Cycle

## Figure 15: Look-Up Table

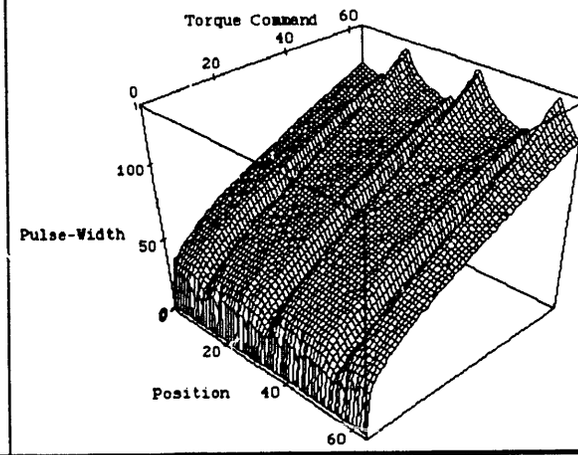


**Legend for Look-Up Tables**

Torque Command Scale: 1=87 oz in
Pulse-Width Scale: 1=1/256% Duty Cycle
Position Scale: 1=1/64 of Full Cycle

## Figure 16: Individual Phase Look-Up Tables

### Phase 1

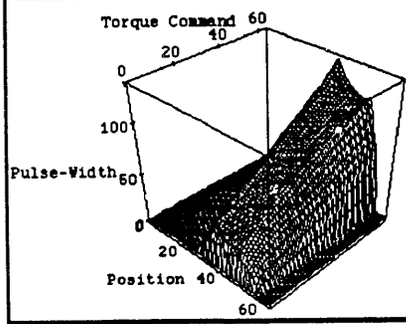


### Phase 2

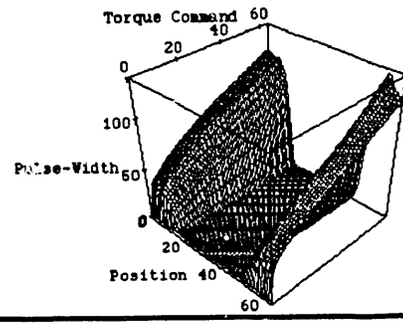


### Phase 3

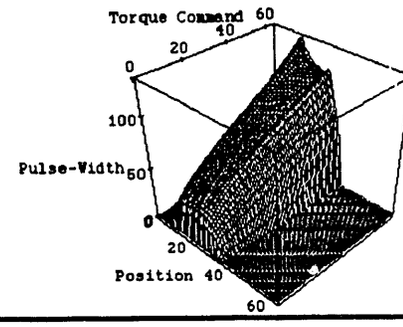

where: p is the position index and P is the maximum table position, c is the command index and C is the maximum command, $\tau_d(p,c)$ is the desired torque, and $\tau(p,c)$ is the actual measured torque. The *pulse-width* is utilized as the command c before compensation and the *torque command* is utilized as the command c after compensation. The desired torque $\tau_d(p,c)$ is computed by fitting a plane to the data. The plane is determined by finding the average torque $\tau_{ave}$ at the half-way contour $c=c_{max}/2$. We compute the plane to pass through the $\{c=0,\ \tau=0\}$ line and the line described by $\{c=c_{max}/2,\ \tau=\tau_{ave}\}$. So, the APMD can be seen as an average torque deviation about the plane of ideal results. This performance measure is equivalent to a digital version of the *torque ripple index* used in [Wallace90a] to quantify torque ripple.

To understand how the APMD varies with command, we average across all positions:

$$CAPMD = \frac{1}{P}\sum_{p=1}^{P}\frac{|\tau_d(p,c)-\tau(p,c)|}{|\tau_d(p,c)|} \qquad \text{for } c=1...C \qquad (2)$$

and for the variation of the APMD with position, we average across all commands:

$$PAPMD = \frac{1}{C}\sum_{c=1}^{C}\frac{|\tau_d(p,c)-\tau(p,c)|}{|\tau_d(p,c)|} \qquad \text{for } p=1...P \qquad (3)$$

*5.4 Torque Linearity Results*

For joints 1 to 4, we plot and compare the results of applying the torque linearization methodology in Figures 17 to 20, respectively. The before (uncompensated) data occupies the left-hand column of plots for each joint, and the after (compensated) data occupies the right-hand column. The *torque* values for joints 1 and 2 have been computed for all plots by multiplying the raw *force* data measurements by the appropriate moment arm. The following 4 plots are shown for each joint before and after compensation:

* The 3-D plot of torque vs position vs command;
* The 2-D plot of PMD distribution;
* The 2-D CAPMD plot; and
* The 2-D PAPMD plot.

The results and some related quantities have also been condensed into tabular form in Table 2.

*5.5 Discussion*

The graphical results for each joint will be discussed in turn beginning with joint 1. The uncompensated torque variations plot for joint 1 displays a periodic torque deviation with position and an exponentially increasing torque with command. The results after compensation are quite linear. The desired wedge shape of the results is indicative of linear performance. From Table 2, we find that the overall uncompensated APMD of 76.1% is reduced to 4.2% after compensation. And, if only the top 90% of the torque range is considered the APMD drops to 1.7%. The percent torque deviations for the lower 10% of the commands increase the APMD for two reasons. First, it is difficult to obtain accurate data at low command values because of the friction in the system. Second, because of quantization, any torque deviation at small command torques represents a large *percentage* deviation. For example, if the torque command is 1 unit and the measured torque is 2 units, the PMD is 100%.

**Table 2: Joint Torque Linearization Results**

| Characteristic | Joint | | | |
|---|---|---|---|---|
| | 1 | 2 | 3 | 4 |
| Motor Type | Var. Rel. | Var. Rel. | Brls. DC | Brls. DC |
| Maximum oz or oz-in (Narrow Ramping) | 7161 | 3966 | 737 | 1215 |
| Maximum oz or oz-in (Wide Ramping) | 10859 | 5546 | 842 | 2521 |
| Increase in Force/Torque Range | 52% | 40% | 14% | 107% |
| Overall APMD (Uncompensated) | 76.1% | 58.3% | 36.0% | 9.1% |
| Overall APMD (Compensated) | 4.2% | 2.4% | 13.1% | 4.6% |
| APMD Improvement Factor | 18.1 | 24.3 | 2.7 | 2.0 |
| APMD Above 10% Command (Compensated) | 1.7% | 1.4% | 12.8% | 2.3% |
| Overall Data Density | 14.8% | 14.0% | 7.9% | 23.0% |
| Percent of Total Torque Range Measured | 50% | 50% | 25% | 100% |
| Data Density in Range | 29.6% | 28.0% | 31.6% | 23.0% |
| Actuation Cycles/Revolution | 150 | 150 | 10 | 10 |
| Table Positions/Actuation Cycle | 512 | 512 | 256 | 256 |
| Table Positions/Degree Motor Rotation | 213 | 213 | 7.1 | 7.1 |
| Phase 1 Equilibrium Position | 341 | 209 | 248 | 79 |

Although many previous works in this field has reported peak torque ripple as a performance measure, we can see from the torque deviation distribution plot that the peak torque deviation is not representative of the overall PMD characteristics. Even though the compensated peak torque deviation is approximately 16% the torque deviation density at this deviation is very low (approximately 1%) and most of the torque deviation density is below 10%. Furthermore,

the deviations plotted here are deviations from the *ideal* torque values; whereas, other works have cited deviations from the *mean* of the data. From the plot of uncompensated CAPMD it is evident that most of the torque deviations are due to deviations of the mean from the ideal mean and not simply deviations of the data from the mean. The average deviation from the ideal value (i.e., the APMD) is more appropriate for characterizing the performance of the torque linearizing methodology.

The torque deviation distribution plot displays how widely varying the torque deviations are. From the uncompensated plot it is evident that PMDs up to 100% are evenly distributed, and the PMDs extend up to 150% at lower proportions. The compensated plot indicates that the linearization methodology has forced all of the deviations down into the range from 0 to 16%. The uncompensated CAPMD plot shows a minimum value half-way up the command range where the plane of desired torque was fit to the data. Due to the friction and quantization, the compensated plot shows high PMDs at low commands.

In the uncompensated PAPMD plot, high PMDs occur for all positions. Moreover, there are peaks in the PMD in the vicinity of the transition regions. The compensated plot shows that the resulting PMDs are much smaller (Notice the scale change between plots) and are uncorrelated with the transition regions.

The joint 2 results shown in Figure 18 are qualitatively the same as those for joint 1 with reduced torque ranges. The uncompensated PMDs in all plots are less than those measured for joint 1, and the compensated results are similar. The APMD is reduced from 58.3% before compensation to 2.4% after, and this reduces to 1.4% if only the top 90% of the command range is considered.

The inherent torque characteristics of the joint 3 brushless DC motor shown in Figure 19 are quite different from those for the variable reluctance motors. The PMD varies greatly with position, showing 6 peaks occurring in the vicinity of the transition regions and in the single phase regions. However, the torque is more linear with pulse-width than for the variable reluctance motors. The compensated plot is less than desired, showing significant PMDs remaining at the original 6 peak positions. The overall APMD is reduced from 36.0% to 13.1%. The original torque deviation distribution shows a wide range of PMDs; none exceeding 100%. Both the CAPMD and the PAPMD plots show reductions of approximately 50% after compensation.

# Figure 17: Joint 1 Torque Linearization Results

**Uncompensated** | **Compensated**

## *Torque Variations*

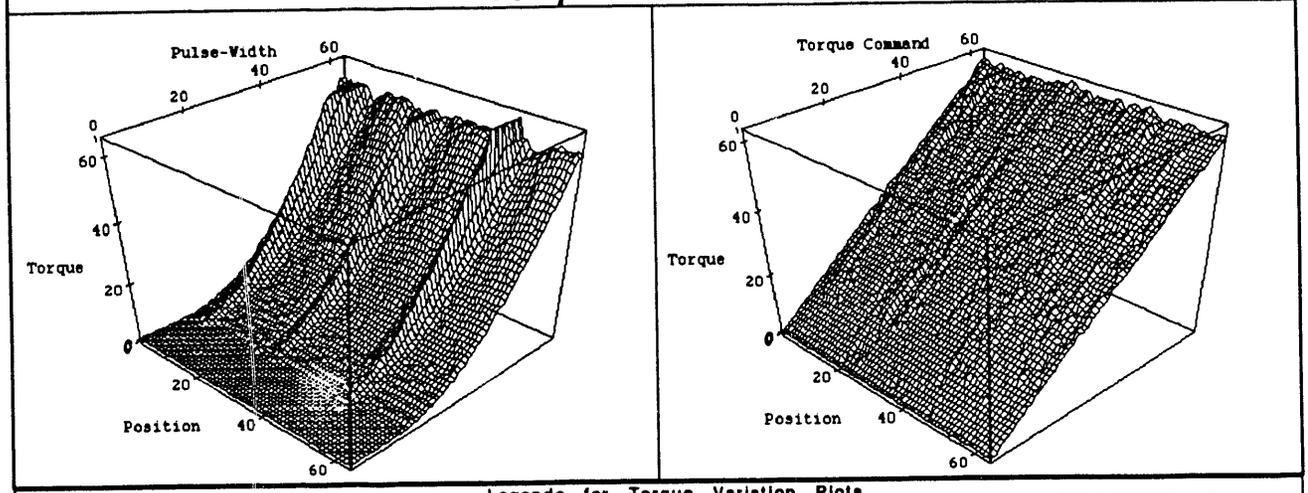


**Legends for Torque Variation Plots**

Pulse-Width Scale: 1=1/128% Duty Cycle
Torque Scale: 1=195 oz in
Position Scale: 1=1/64 of Full Cycle

Torque Command Scale: 1=173 oz in
Torque Scale: 1=173 oz in
Position SCale: 1=1/64 of Full Cycle

## *Torque Deviation Distribution*

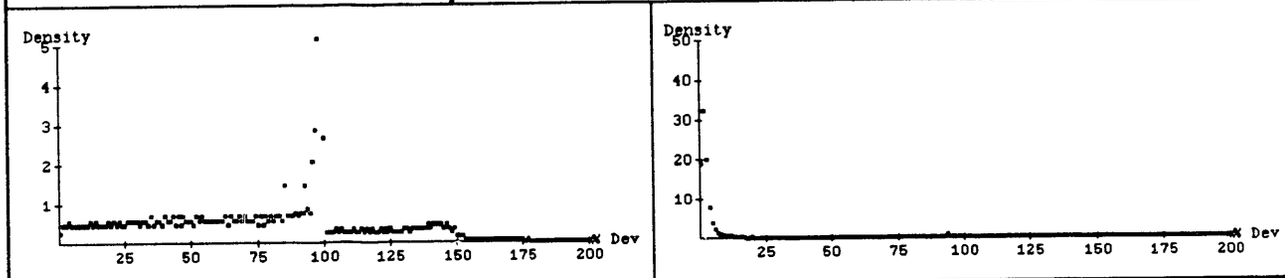


## *Torque Deviations with Command*

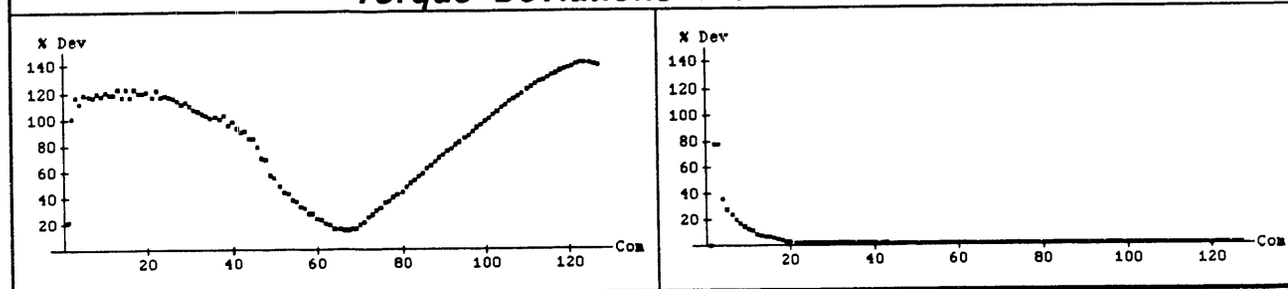


## *Torque Deviations with Position*

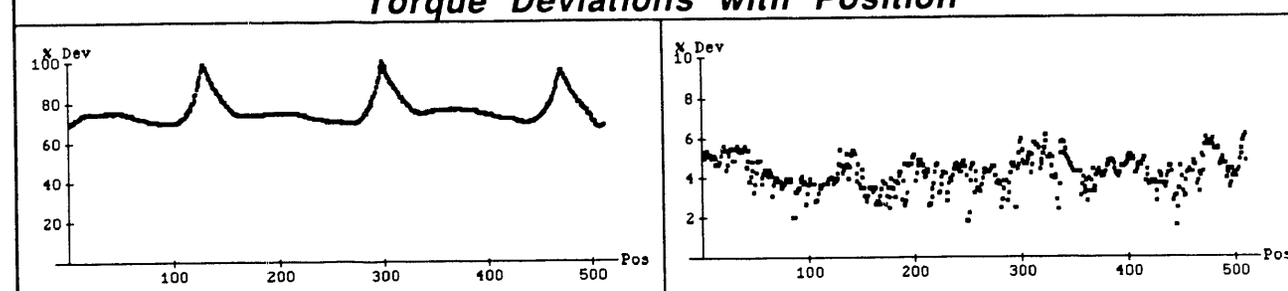


**Legend for Torque Deviation Plots**

Density : Density of Torque Deviation as a Percentage of the Total
% Dev : Percent Torque Deviation; i.e., |Torque Deviation|/Torque Command
Com : Command (Pulse-Width and Torque, Respectively)
Pos : Position ..... 1=1/512 of Full Cycle

# Figure 18: Joint 2 Torque Linearization Results

**Uncompensated** | **Compensated**

## *Torque Variations*

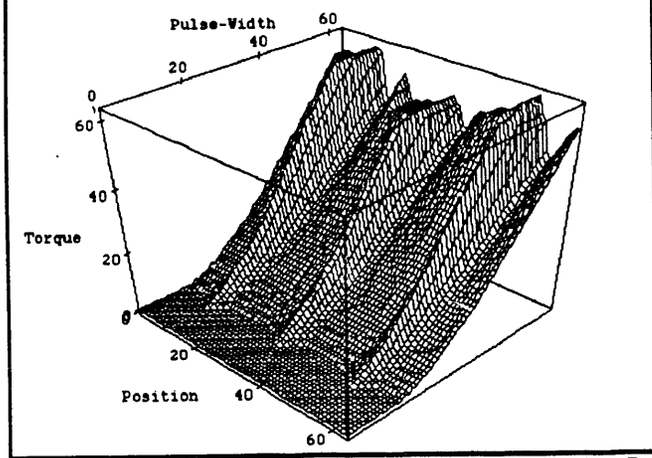


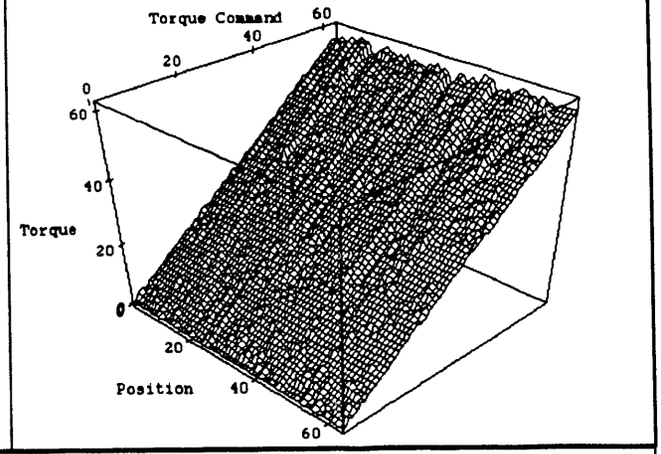


**Legends for Torque Variation Plots**

Pulse-Width Scale: 1=1/128% Duty Cycle
Torque Scale: 1=114 oz in
Position Scale: 1=1/64 of Full Cycle

Torque Command Scale: 1=87 oz in
Torque Scale: 1=87 oz in
Position SCale: 1=1/64 of Full Cycle

## *Torque Deviation Distribution*

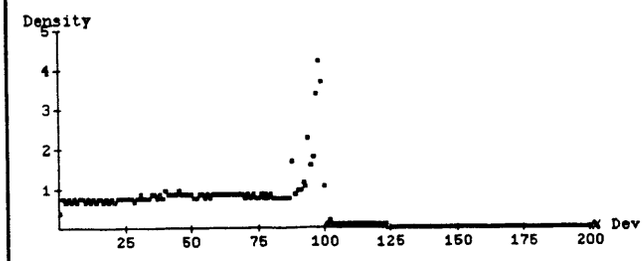


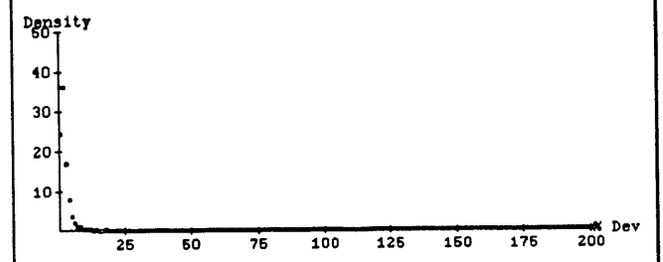


## *Torque Deviations with Command*

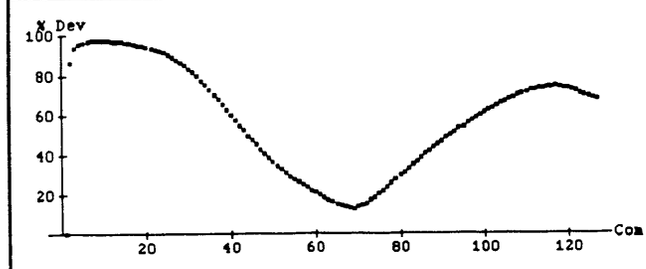


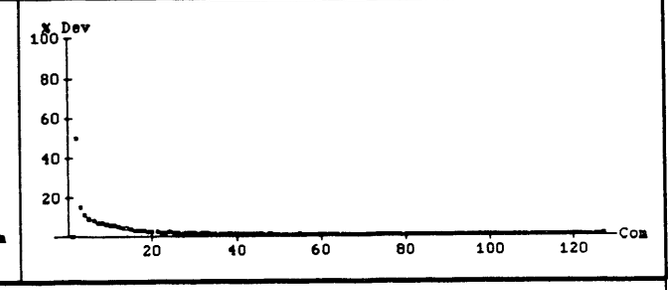


## *Torque Deviations with Position*

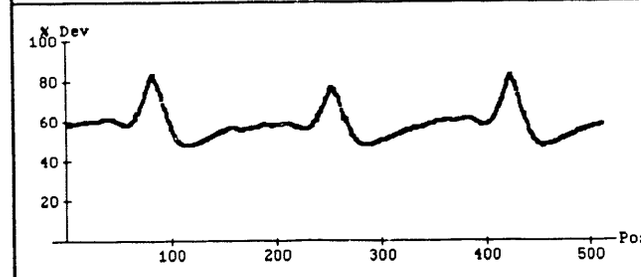


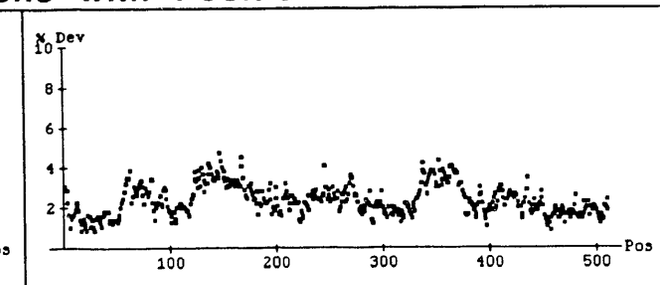


**Legend for Torque Deviation Plots**

Density : Density of Torque Deviation as a Percentage of the Total
% Dev : Percent Torque Deviation; i.e., |Torque Deviation|/Torque Command
Com : Command (Pulse-Width and Torque, Respectively)
Pos : Position ..... 1=1/512 of Full Cycle

# Figure 19: Joint 3 Torque Linearization Results

**Uncompensated** | **Compensated**

## *Torque Variations*

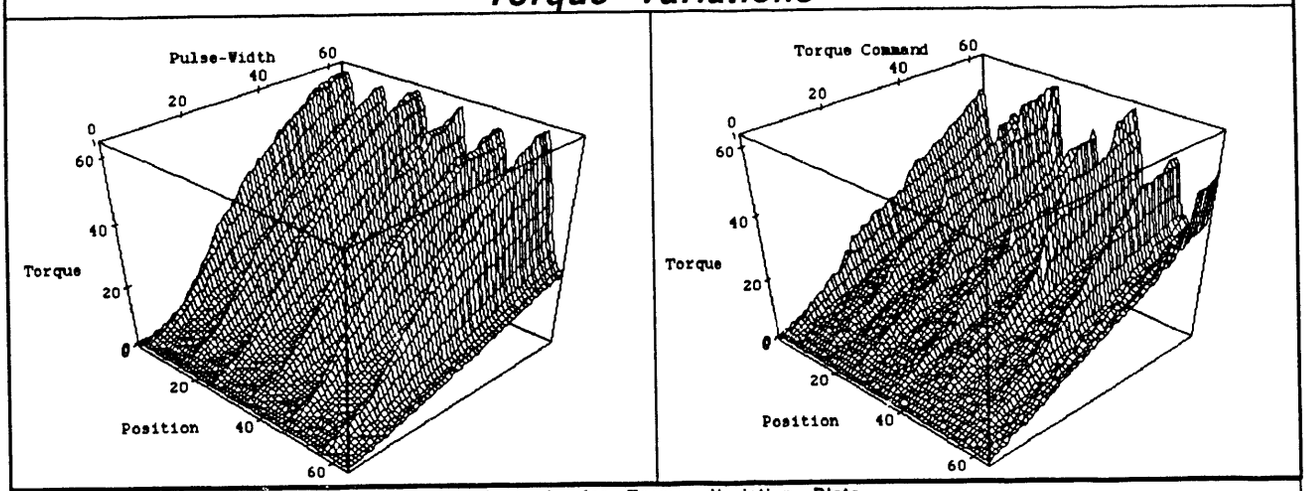


**Legends for Torque Variation Plots**

Pulse-Width Scale: 1=1/128% Duty Cycle
Torque Scale: 1=195 oz in
Position Scale: 1=1/64 of Full Cycle

Torque Command Scale: 1=173 oz in
Torque Scale: 1=173 oz in
Position SCale: 1=1/64 of Full Cycle

## *Torque Deviation Distribution*

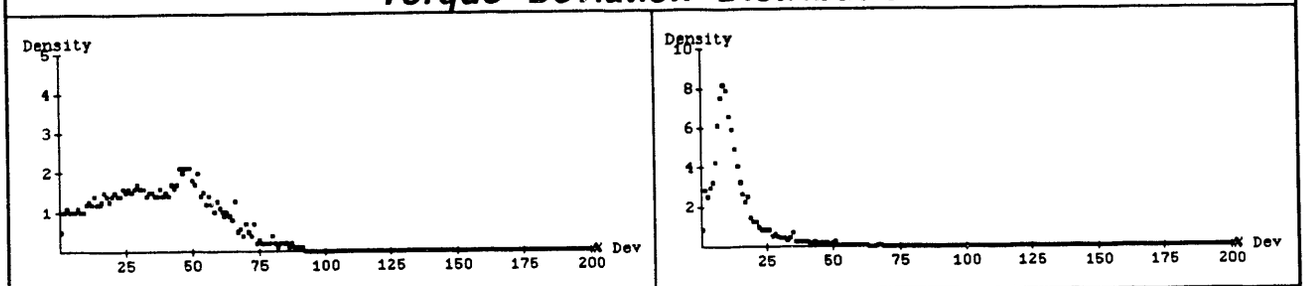


## *Torque Deviations with Command*

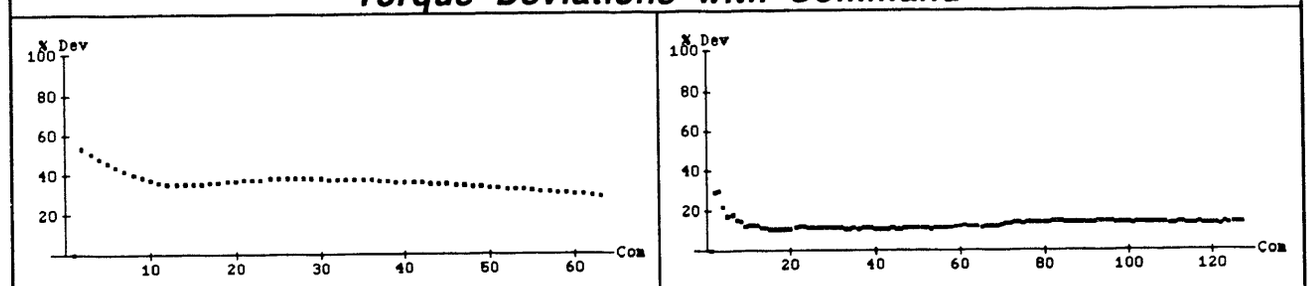


## *Torque Deviations with Position*

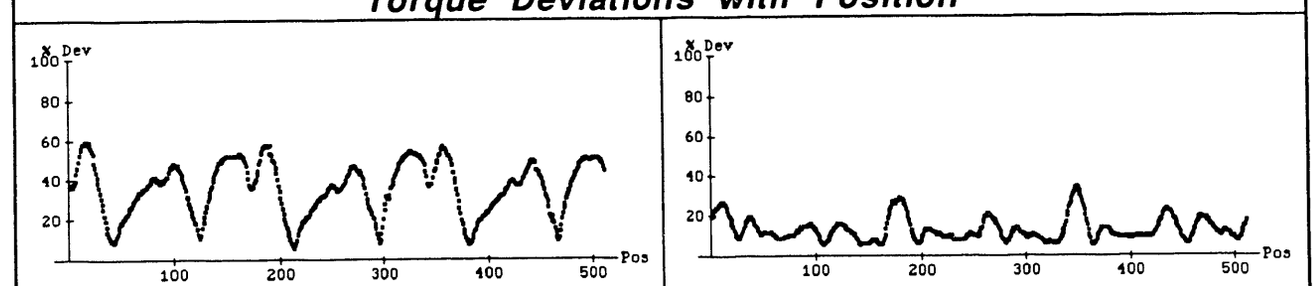


**Legend for Torque Deviation Plots**

Density : Density of Torque Deviation as a Percentage of the Total
% Dev : Percent Torque Deviation; i.e., |Torque Deviation|/Torque Command
Com : Command (Pulse-Width and Torque, Respectively)
Pos : Position ..... 1=1/512 of Full Cycle

# Figure 20: Joint 4 Torque Linearization Results

**Uncompensated** | **Compensated**

## *Torque Variations*

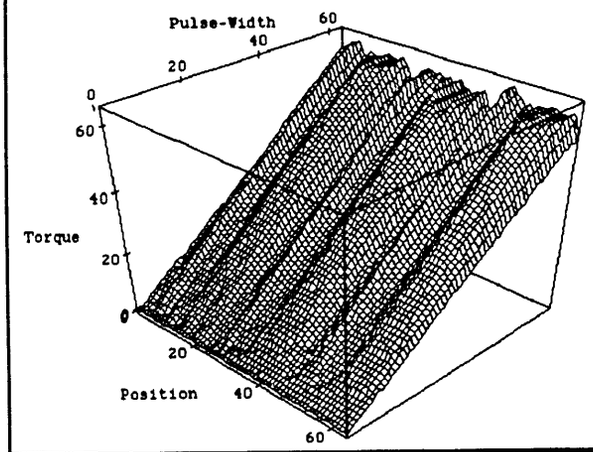


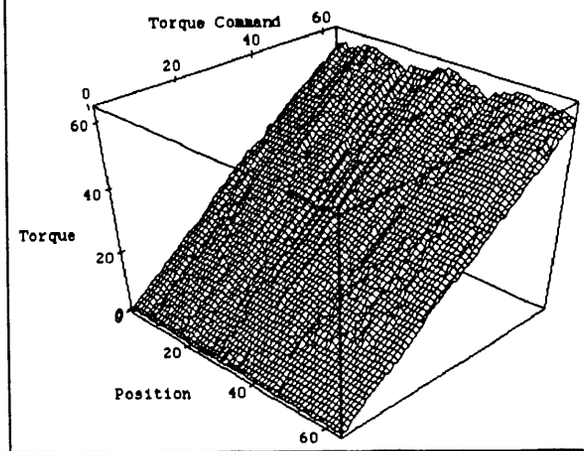


**Legends for Torque Variation Plots**

Pulse-Width Scale: 1=1/64% Duty Cycle
Torque Scale: 1=47 oz in
Position Scale: 1=1/64 of Full Cycle

Torque Command Scale: 1=41 oz in
Torque Scale: 1=41 oz in
Position SCale: 1=1/64 of Full Cycle

## *Torque Deviation Distribution*

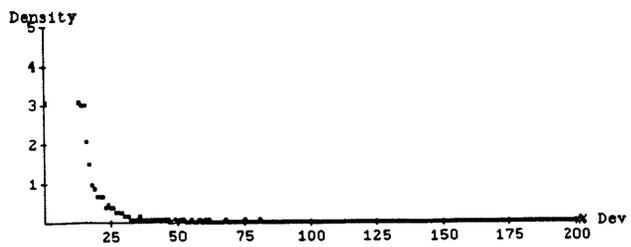


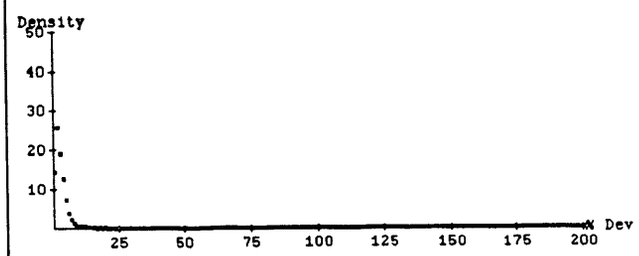


## *Torque Deviations with Command*

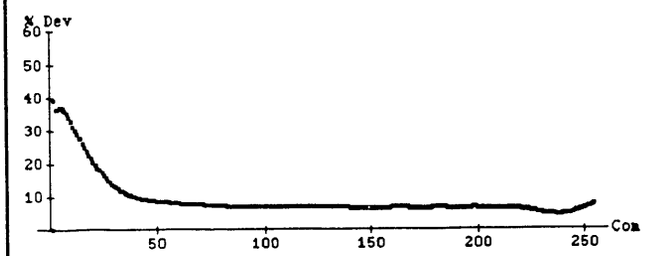


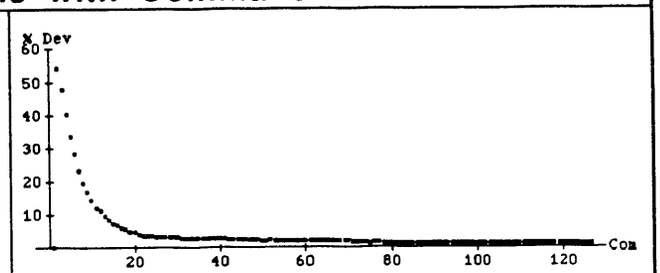


## *Torque Deviations with Position*

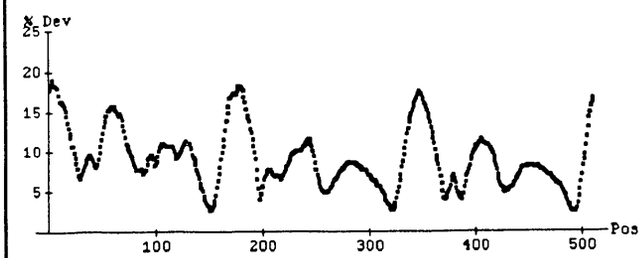


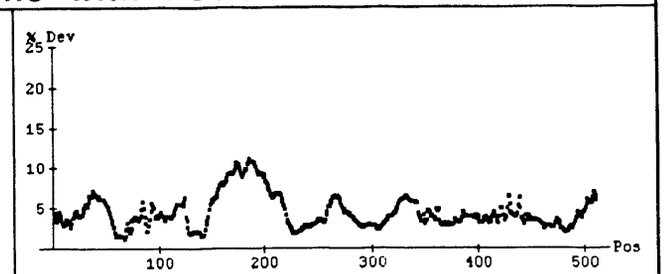


**Legend for Torque Deviation Plots**

Density : Density of Torque Deviation as a Percentage of the Total
% Dev : Percent Torque Deviation; i.e., |Torque Deviation|/Torque Command
Com : Command (Pulse-Width and Torque, Respectively) Full Range Shown
Pos : Position ..... 1=1/512 of Full Cycle

The uncompensated joint 4 torque characteristics are quite linear. As compared to the two previous variable reluctance motors, and the joint 3 brushless DC motor, joint 4 shows less PMDs with position and command. Its inherent torque deviation distribution is confined to the 0-30% range. The linearization methodology improves the performance as is shown in the compensated plots. The APMD is reduced from 9.1% before compensation to 4.6% after, and this reduces to 2.3% if only the top 90% of the command range is considered. The torque deviation is not reduced by as much as for joints 1 and 2 because the look-up table positions are quantized much coarser: 7.1 positions/degree for joints 3 and 4 compared with 213 positions/degree for joints 3 and 4 as shown in Table 2.

### *5.6 An Unexpected Phenomenon*

An unexpected phenomenon was observed during the data collection experiments. A mechanical oscillation between the force sensor and the constraint occurred at intermittent times producing an audible buzzing sound but inperceptible motion. The cause of the oscillation was traced to the interaction between special table configurations and the system compliance.

It is easiest to describe the effect by an example. Consider incrementally increasing the torque command while a joint motor is being driven to press against a constraint. Initially, the motor is exerting some torque and the robot and constraint are complying according to Hooke's law (i.e., $\Delta x = f/k$, where $\Delta x$ is the position displacement, f is the force and k is the combine stiffness). When the torque command is increased by one unit, the next higher address in the look-up table is indexed to retrieve the next pulse-width during the next table look-up cycle. The new pulse-width will be *larger*, in general, than the previously applied pulse-width. So the motor will exert a slightly larger torque and the robot and constraint will comply proportionately more. The compliance causes a small differential change in motor position to the next position unit. So, during the next table look-up cycle the new position is used to index into the table at the same torque command. If this new pulse-width entry is *less* that the current pulse-width, the motor will exert *less* torque than before. The reduction in torque will cause the system to comply less and the position will *change back* to the original position. With the same torque command at the original position, the previous higher pulse-width value is again retrieved and applied during the succeeding table look-up cycle. This cycle repeats itself producing the high frequency oscillation. Because the oscillations are caused by motions between adjacent table positions, the amplitude of the

oscillations is inperceptibly small (e.g., one table position increment = 0.005° for joint 1) and the frequency is likely an even divisor of the JIB operating frequency (e.g., 10Khz).

According to the procedure described in Section 4 for assembling the look-up tables, pulse-width entries can naturally be smaller or larger than their neighbors at the same torque command but different position. So the circumstances producing the oscillations are an inherent property of the table look-up approach. However, a method has been identified which reduces their occurrence. When inspecting the look-up tables to understand the cause of the oscillations, some table entries were found to be non-monotonically increasing. That is, when scanning through the look-up table at a constant position in the direction of increasing torque command, some pulse-widths were discovered which were not equal or greater than the previous pulse-widths. This is inappropriate since larger torques always require larger pulse-widths at the same position. To correct the problem and ensure monotonically increasing pulse-widths, a program was developed to filter the look-up tables. The program scans each look-up table looking for non-monotonically increasing pulse-widths and replaces each bad entry by the previous pulse-width value at the current position.

After applying this correction function, the occurrences of the oscillations during the data collection experiments were less frequent. It should be noted that during servo control of the joints under torque commands, the oscillation phenomenon has not been detected. It appears that when the torque commands are varied at servo rates, the oscillations do not occur. Thus, the oscillation phenomenon is not expected to require special consideration in systems when a closed-loop servo is implemented.

## 6. Conclusions

### *6.1 Summary*

A practical methodology has been developed to linearize the joint torque characteristics for a commercial electric direct-drive robot. The methodology was applied to the commercial Adept II robot through the construction of special purpose joint interface boards. The torque deviations were significantly reduced for both variable reluctance and brushless DC motors. The torque deviations for the direct-drive joints are reduced to below 5% and if only the upper 90% of the command range is considered, the torque deviations are

below 2.5%. The methodology reduced torque deviations for the ball-screw driven joint by approximately 50%.

The methodology is generalized to any electric motor/amplifier combination having position feedback. The linearization procedure requires no manual operation, no high accuracy measuring devices, no a priori models of either the motors or the amplifiers and no accurately machined fixtures. This makes it a practical, economical approach amenable to commercial application.

### *6.2 Methodology Enhancements*

Some enhancements to the methodology for which there is insufficient time to pursue have become apparent. Perhaps the motor characteristics obtained in this study can be used for other motors without conducting the time consuming data collection experiments. We suggest that it may be possible to collect a handful of characteristic parameters from a new motor (e.g., phase equilibrium positions, and the torques at the middle of the three transition regions and at the middle of the single phase regions). These parameters could then be applied to modify the existing data of the same motor type by means of systematic scaling to obtain look-up tables without the 4 hour data collection procedure. Such an approach may produce slightly inferior results but the reduction of characterization time would be a great practical advantage.

It should be easier to linearize the motor torques before they have been mounted into the robot structure. This suggests a new set of products directed towards robotics and automation market sectors. Motor manufacturers could have a special product line for robotics applications. The new product line would simply be their current motors which have been fully characterized. The manufacturer would conduct data collection experiments on each motor and supply this data with the motor at an added cost. An original equipment manufacturer could then purchase these pedigreed motors and combine each with an amplifier, position sensor and torque compensator utilizing our torque linearization methodology. The resulting new product could be marketed as a high accuracy "virtual torque actuator" for robotics applications. Robot builders can then purchase the virtual torque actuators as a single component and simplify their robot designs. Finally, robot end users would have available a new series of robots which provide enhanced performance for the new and growing automated assembly and light machining industries.

A trade-off exists in the digital control of robots. For in-contact robot applications, high resolution of applied forces at low force

values is desired. However, for fast, free-space motions, high torques are required but low resolution is sufficient. Thus, both high torque and high resolution are desirable characteristics for robot control. Because of the fixed ranges for control variables in digital implementations (e.g., 8-bit quantities allow only 256 possible values), we cannot obtain both high resolution and high torque ranges. By conventional methods, when the torque range is increased, the resolution drops and visa versa. However, we can remedy the situation within the look-up tables of the joint torque linearization methodology. The torque command range can be logarithmically scaled when the tables are computed. Then, at the next higher control level, the torque commands are exponentially scaled before commanding the JIBs. The exponential operation cancels the logarithmic scaling to produce linear torques as before. However, now we have an actuator with high resolution at low torques and low resolution at high torques as desired.

### *6.3 Continuing Work*

Beyond demonstrating the torque deviation reductions, we have characterized the variations of the torque deviations with position and command. These deviation models can now be used in the development of future high performance robot controllers.

Fundamentally, linearizing the torque characteristics removes uncertainty in the system and thereby enhances performance. Linear joint torque command capability shows promise to allow increased speed during in-contact operations. Technology transfer from robot control to the commercial and industrial communities will also be facilitated. The Adept II robot of this work is now being utilized as a testbed to demonstrate the potential of applying linear joint torque commands for increasing the speed of in-contact robot control operations while maintaining stability.

## 7. Acknowledgements

This work was performed at Sandia National Laboratories and was supported by the U.S. Department of Energy under Contract DE-AC04-76DP00789. We gratefully acknowledge Jon Bryan of the Intelligent Machine Principles Division of Sandia National Laboratories for the design and construction of the JIBs.

## 8. Bibliography


[Asada85] H. Asada and S. Lim, "Design of Joint Torque Sensors and Torque Feedback Control for Direct-Drive Arms," in Proceedings of the ASME Winter Annual Meeting, Miami, FL, November 1985.

[Asada87] H. Asada and K. Youcef-Toumi, *Direct Drive Robots: Theory and Practice*, The MIT Press, Cambridge, MA, 1987.

[Curran85] R. Curran and G. Mayer, "The Architecture of the AdeptOne Direct-Drive Robot," *Proceedings of the 1985 American Control Conference*, Boston, MA, June 1985, pp. 716-721.

[Hogan84] N. Hogan, "Impedance Control: An Approach to Manipulation: Part I-Theory, Part II-Implementation, and Part III-Applications," *Proceedings of the 1984 American Control Conference*, CA, June 1984, pp. 304-313.

[Ish-Shalom89] J. Ish-Shalom, "Experimental Results of Using a Linear Step Motor as a Programmable Spring," *Proceedings of the 1989 IEEE International Conference on Robotics and Automation*, Scottsdale, AZ, May, 1989, pp. 1841-1846.

[Luh80] J.Y.S. Luh, M.W. Walker and R.P.C. Paul, "Resolved-Acceleration Control of Mechanical Manipulators," *IEEE Transactions on Automatic Control*, Vol. AC-25, No. 3, June 1980, pp. 468-474.

[Luh83] J.Y.S. Luh, W.D. Fisher and R.P. Paul, "Joint Torque Control by a Direct Feedback for Industrial Robots", *IEEE Transactions on Automatic Control*, Vol. AC-28, No. 2, February 1983, pp. 153-161.

[Markiewicz73] B.R. Markiewicz, "Analysis of the Computed Torque Drive Method and Comparison with Conventional Position Servo for a Computer-Controlled Manipulator," Jet Propulsion Laboratory Technical Memo No. 33-601, Los Angeles, CA, March 1973.

[Newman91] W.S. Newman and J.J. Patel, "Experiments in Torque Control of the AdeptOne Robot," *Proceedings of the 1991 IEEE International Conference on Robotics and Automation*, Sacramento, CA, April 1991, pp. 1867-1872.

[Patel90] J. Patel, *Torque Control and Modeling of the AdeptOne Robot*, Master's Project Report, Department of Electrical Engineering and Applied Physics, Case Western Reserve University, May 1990.

[Paul72] R.C. Paul, "Modelling, Trajectory Calculation and Servoing of a Computer Controlled Arm," A.I. Memo 177, Stanford Artificial Intelligence Laboratory, Stanford University, September 1972.

[Pfeffer86] L. Pfeffer, O. Khatib and J. Hake, "Joint Torque Sensory Feedback in the Control of a Puma Manipulator," *Proceedings of the 1986 American Control Conference*, Seattle, WA, June 1986, pp. 818-824

[PMI88] PMI Motion Technologies, *Motion Control Components Catalog*, 49 Mall Drive, Commack NY, 11725-5703,1988.

[Raibert81] M.K. Raibert and J.J. Craig, "Hybrid Position/Force Control of Manipulators," *Journal of Dynamic Systems, Measurement, and Control*, Vol. 102, June 1981, pp. 126-133.

[Salisbury80] J.K. Salisbury, "Active Stiffness Control of a Manipulator in Cartesian Coordinates," *Proceedings of the 19th IEEE Conference on Decision and Control*, December 1980, pp. 95-100.

[Starr90] G.P. Starr and C.W. Wilson, "Design of a Torque Controller for the Adept-2 Robot", *Proceedings of the Third International Symposium on Robotics and Manufacturing*, Burnaby, British Columbia, Canada, July 1990, pp. 299-306.

[Taylor86] D.G. Taylor, M. Ilic-Spong, R. Marino and S. Peresada, "A Feedback Linearizing Control for Direct Drive Robots with Switched Reluctance Motors," Proceedings of the 25th IEEE Conference on Decision and Control, Athens, Greece, December 1986, pp. 388-396.

[Taylor88] D.G. Taylor, M.J. Woolley and M. Ilic, "Design and implementation of a linearizing and decoupling feedback transformation for Switched Reluctance Motors," Proceedings of the 17th Symposium on Incremental Motion Control Systems and Devices, Champaign, Illinois, June 1988, pp. 173-184.

[Vertal89] M.D. Vertal, *Development of a Torque Controller for the AdeptOne Robot*, Master's Project Report, The Department of Electrical Engineering and Applied Physics, Case Western Reserve University, May 1989.

[Wallace90a] R.S. Wallace and D.G. Taylor, "Torque Ripple Reduction in Three-Phase Switched Reluctance Motors," *Proceedings of the American Control Conference*, San Diego, CA, May 1990.

[Wallace90b] R.S. Wallace and D.G. Taylor, "A Balanced Commutator for Three-Phase Switched Reluctance Motors to Minimize Torque Ripple," *Proceedings of the IEEE International Conference on Systems Engineering*, Pittsburgh, PA, August 1990, pp. 597-600.

[Whitney85] D.E. Whitney, "Historical Perspective and State of the Art in Robot Force Control," Proceedings of the 1985 IEEE International Conference on Robotics and Automation, St. Louis, MO, 1985, pp. 262-268.

[Yoshikawa88] T. Yoshikawa, T. Sugie and M. Tanaka, "Dynamic Hybrid Position/Force Control of Robot Manipulators-Contoller Design and Experiment," *IEEE Journal of Robotics and Automation*, Vol. 4, No. 6, December 1988, pp. 699-705.

## Distribution

1400 E.H. Barsis

1410 P.J. Eicker

1414 R.W. Harrigan

1416 A.T. Jones

1411 P.F. Muir (15 copies)

1411 Dolores Miller (15 copies for 1410 Library)

1411 J.R. Bryan

1411 G.P. Starr

3141 S.A. Laudeuberger (5 copies)

3145 Document Processing for DOE/OST1 (8 copies)

3151 G.C. Claycomb

3523-2 Central Technical Files

# END

# DATE FILMED

11/14/91